Synthesis and Characterization of Oriented MFI Membranes Prepared by Secondary Growth

Mark C. Lovallo, Anastasios Gouzinis, and Michael Tsapatsis
Dept. of Chemical Engineering, University of Massachusetts, Amherst, MA 01003

MFI membranes were prepared as free-standing and supported films on porous alumina disks and nonporous substrates. They were synthesized using secondary growth of precursor layers. For self-supported films the first step was to prepare an alumina–silicalite composite film, while for supported films the substrate was first coated with layers of the nanocrystalline silicalite particles. During the following hydrothermal treatment, silicalite particles acting as seed crystals form a dense film, which consists of 0.5–100-μm-thick columnar, intergrown, preferentially oriented grains. The crystal orientation of the MFI films was examined using X-ray diffraction pole-figure texture analysis. The crystals were preferentially oriented with both sinusoidal and straight channel networks along directions nearly parallel to the membrane surface. The degree of orientation increased with increasing membrane thickness. Single gas permeances through thin, oriented membranes were measured. Apparent activation energies for permeation were 16, 24, 30, 22 and 26 kJ/mol for H_2, N_2, O_2, CH_4, and CO_2, respectively. Ideal selectivities for H_2/N_2, CO_2/CH_4, and O_2/N_2 were as high as 30, 10, and 3.5, respectively. Binary permeation measurements for the gas pairs CO_2/CH_4, O_2/N_2, and CO_2/N_2 revealed trends similar to those of single gas permeation and the properties are attributed to the membrane microstructure.

Introduction

During the past decade, the preparation of zeolite membranes has been reported for several zeolite structure types (Tsikoyiannis and Haag, 1992; Geus et al., 1992; Jia et al., 1993; Noble and Falconer, 1995; Vroon et al., 1996; Yan et al., 1995; Kapteijn et al., 1995; Bakker et al., 1996; Kusakabe et al., 1997). However, reproducible control over membrane microstructure (i.e., thickness, grain size, crystal orientation) has been limited. To obtain optimal zeolite membranes the development of a flexible technique allowing for control over film and membrane characteristics is desirable.

In 1994, we proposed and reported on the use of colloidal zeolite suspensions for precursor film casting followed by secondary growth for zeolite membrane formation (Tsapatsis et al., 1995a). Our group has used this technique to prepare zeolite films and membranes of several different morphologies and structure types: zeolite L (Lovallo et al., 1996a; Tsapatsis et al., 1995b), MFI (Lovallo and Tsapatsis, 1996; Lovallo et al., 1996b), and zeolite A (Boudreau and Tsapatsis, 1997). Figure 1 outlines the methodology for producing these films.

Fabrication begins with the casting of a precursor film. The film can be either supported by dip/spin coating or self-supported by evaporation of the solvent in a casting dish. For the case of zeolite L, the self-supported precursor film is composed of randomly oriented crystals. Secondary growth proceeds through a gel phase, resulting in a thin and randomly oriented asymmetric zeolite L film.

MFI films and membranes have also been fabricated from randomly oriented precursor films. However, we have identified conditions where secondary growth occurs in a preferred direction, producing a thin and preferentially oriented MFI layer.

For zeolite A, preparation of an oriented precursor layer was achieved by depositing cube-shaped crystals face down on a substrate. The orientation of the dense and thin film formed after secondary growth was attributed to the orienta-

Correspondence concerning this article should be addressed to M. Tsapatsis

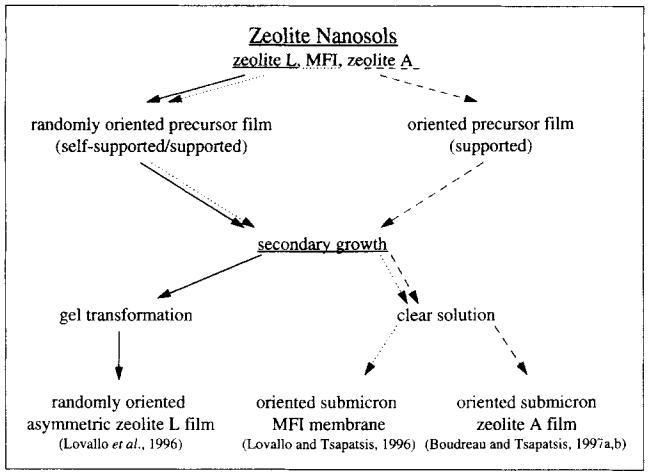

Figure 1. Zeolite film and membrane processing methodology.

tion of the precursor film, in contrast to the MFI layer, where the preferred orientation was a result of crystal growth.

These three cases demonstrate the flexibility of the secondary growth technique. Compared to previous *in-situ* methods for zeolite film and membrane formation, a greater command over final film microstructure (thickness, degree of orientation) can be achieved. The presence of an already formed precursor film allows for implementation of a wider range of hydrothermal synthesis conditions leading to formation of continuous films. This method provides added flexibility in selecting deposition conditions for tailoring film microstructure because the constraints imposed by the need for film nucleation can be relaxed in favor of synthetic conditions imposed by the desired film texture and thickness.

A similar approach has also recently been reported by Valtchev et al. (1996) and Mintova et al. (1997) for producing hollow fibers of silicalite and ZSM-5 films supported on gold surfaces. The method employs surface modification to facilitate the adsorption of zeolite seed crystals on the substrate followed by a seeded growth (what we term secondary growth). No preferred orientation or permselectivity has been demonstrated for these films. Also, in a number of patent applications, researchers at Exxon have proposed the use of small zeolite particles for the deposition of a growth enhancing layer (GEL) which is hydrothermally treated to form a membrane (Lai et al., 1996). Preferred orientation was demonstrated and a wide variety of possible separations has been claimed in this patent application.

We have reported on the permeation characteristics of self-supported, submicron, and preferentially-oriented MFI membranes (Lovallo and Tsapatsis, 1996). Some of the permeation properties of the membranes include ideal selectivities as high as 60 for H_2 over N_2 and as high as 3.6 for O_2 over N_2. Apparent activation energies for H_2, N_2, and O_2 were found to be 11, 26, and 32 kJ/mol, respectively. The overall size of the zeolite membranes reported was limited to the size of the self-supported precursor silicalite film (typically a few cm in diameter). For practical applications, large membrane areas are needed. This can be accomplished by preparing similar zeolite membranes supported on porous inorganic substrates.

In what follows we describe the extension of the secondary growth technique for the preparation of oriented, thin MFI molecular sieving layers supported on commercially available macroporous alumina disks. The permeation characteristics of the supported membranes are presented and closely correspond to the results previously reported for the self-supported membranes. Having established the extension of the technique to supported membranes on macroporous substrates, we also report binary permeation data and further characterize the microstructure and growth mechanism of the membranes using X-ray pole-figure analysis, energy dispersive spectroscopy (EDAX), electron probe microanalysis (EPMAX), and scanning electron microscopy (SEM).

Experimental Procedure

Membrane preparation

A colloidal suspension of silicalite particles approximately 100 nm in size was prepared according to the procedure previously reported by Lovallo and Tsapatsis (1996). Repeated washing, centrifugation of the particles, and dilution with deionized water was used to adjust the concentration and pH of the aqueous suspension to 20-g silicalite/L and pH ~ 8.

Self-Supported Membranes. The colloidal suspension of silicalite particles was used to prepare a precursor self-supported film by evaporation of the solvent (water) in a petri dish. An alumina binder was added to the suspension to increase the chemical and mechanical stability of the films. The self-supported films were opaque and typically ~ 1 mm thick with a 1-cm diameter. These self-supported films were calcined at 550°C and subsequently exposed to a hydrothermal secondary growth treatment (Lovallo and Tsapatsis, 1996). Recovered films were washed in deionized water and calcined at 550°C for several hours.

Supported Membranes. Porous α-alumina substrates (3 cm in diameter and 0.5 cm thick) were obtained from Coors. The porous disks had an average pore diameter of ~ 0.5 μm and an apparent porosity of 19.6%. The substrates were polished in several steps until a smooth shiny surface was observed. The substrates were examined by inspection under an optical microscope for any large defects (scratches, cracks, chips). The porous disks were then washed in a 0.1-M HNO_3 bath for several hours before being washed with deionized water until a pH of ~ 7 was attained.

The porous disks were then vertically placed into the silicalite suspensions and remained immersed for several minutes. The disks were vertically removed from the suspensions at a rate of 1 cm/s and dried in air at room temperature. The process was repeated as many times as needed to form precursor films of various thicknesses. The coated disks were calcined at 500°C and postprocessed according to the secondary growth procedure (Lovallo and Tsapatsis, 1996). After secondary growth the supported films were washed in deionized water and then calcined at 550°C for several hours.

Supported Films on Nonporous Substrates. To investigate the mechanism of secondary growth, films were also prepared on nonporous microscope glass slides. The substrates were coated with the precursor film before being calcined at 500°C and exposed to hydrothermal treatment for secondary growth. In some cases the calcination step and the use of the alumina binder were omitted from the formation of the pre-

cursor layer in order to investigate the effects on the subsequent secondary growth. Due to the glass slides' relatively flat surface, quantitative characterization of the degree of orientation by X-ray diffraction (XRD) is possible.

X-ray diffraction

XRD patterns of supported films were collected on a Phillips X'Pert using CuKα radiation. Supported films on glass slides were analyzed with the film surface perpendicular to the plane of the X-ray source and detector. In this diffractometer geometry, only crystal planes that are parallel or nearly parallel to the film surface contribute to the XRD pattern.

Additional orientation analysis was performed using pole-figure measurements. For these experiments the 2θ position corresponding to the desired crystal plane was identified from the standard (θ–2θ) XRD pattern of the films supported on glass slides. The pole-figure measurement was then made by placing the detector and source at the position of the associated peak. This position does not change during the pole-figure measurement. During the pole-figure data collection the sample is rotated 360° (ϕ) for each tilt angle ψ. For these experiments the sample was tilted from 0° ψ (film surface perpendicular to the plane of the X-ray source and detector) to 80° ψ (film surface nearly parallel to the plane of the source and detector). This type of analysis allows for the determination of texture or preferred orientation of the supported film.

A similar analysis was performed on an MFI membrane with a randomly oriented surface layer. The membrane was prepared according to the report of Yan et al. (1995). The data from this randomly oriented sample were used to correct the pole-figure data for defocusing effects (intensity reduction due to X-ray beam defocus during sample tilting) (Huijser-Gerits and Rieck, 1974).

SEM, EDAX, and EPMA

SEM and EDAX were performed on a JEOL 6320FXCV field emission-scanning electron microscope (FE-SEM) operating at 10 kV equipped with a lithium light element detector. Samples were carbon coated prior to examination. EPMA was also performed on selected samples in order to make use of the lower detection limits for Na and Al provided by wavelength dispersive spectroscopy (WDS).

Gas permeation measurements

Single gas permeances through calcined, supported MFI membrane were measured for several gases. The membrane was attached to a glass tube with an epoxy. The exposed membrane area was ~1 cm in diameter. The permeate side of the membrane was held under vacuum while the desired gas was passed over the feed side of the membrane at atmospheric pressure. After equilibration the permeate side was isolated from vacuum and the rate of change in permeate side pressure was monitored up to 3 torr (400 Pa). Permeances were calculated based on the pressure differential, the permeate side dead volume, the membrane area, and the rate of pressure change. Permeances at several temperatures were measured for all gases.

For mixed gas permeation measurements self-supported MFI membranes were attached to the end of the glass tube with an epoxy. A Wicke-Kallenbach configuration was employed where the mixed feed was introduced in the feed side of the membrane at 50–100 cm^3/min and a sweep gas was fed through a 1/16-in. (1.6-mm) capillary tube to the surface of the membrane. The sweep rate was varied between 2–10 cm^3/min. The sweep with permeate was directed to a 1 cm^3 sample loop which could be switched to feed the sample to a Hewlett-Packard Series 5890 gas chromatograph (GC). A thermal conductivity detector was used in all cases with a molecular sieve packed column for experiments with the O_2/N_2 mixtures and a Chromosorb 80/100 packed column for CO_2/N_2 and CO_2/CH_4 measurements. Several hours were allowed between measurements, as necessary, in order to ensure equilibration when the feed side composition was changed. The GC data were used to determine feed and permeate compositions as well as permeances.

Results and Discussion

Microstructural characterization and growth process

Figure 2 shows a pole-figure line plot (after defocus correction) for the (101) and (501) crystal planes of the supported MFI film. The figure shows the diffracted X-ray intensity vs. sample tilt angle (ψ). For a film of randomly oriented crystals, tilting (or spinning) the sample will have no effect on the corrected X-ray intensity. Previous analysis showed that spinning the sample had no effect on diffracted intensity (Lovallo and Tsapatsis, in press). This indicates random rotation of the MFI crystals around the axis perpendicular to the membrane surface as expected by visual observation of SEM micrographs. For this reason, the pole-figure line plots of Figure 2 are sufficient for determining the orientation aspects of the film and can be viewed as providing the distribution of orientation of the corresponding crystallographic planes with respect to the substrate surface.

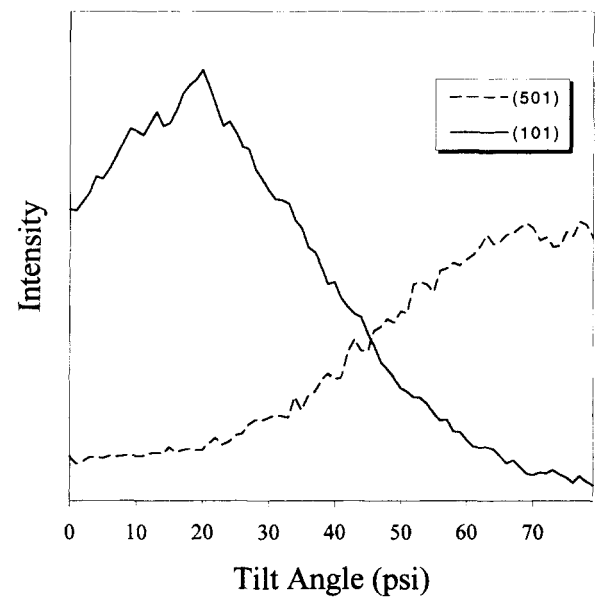

Figure 2. XRD pole-figure analysis of MFI film for (101) and (501) MFI crystal planes.

The (101) line plot in Figure 2 shows considerable intensity at a 0° tilt angle and a maximum intensity at around a 20° tilt angle. In contrast, the (501) line plot shows almost no intensity at a 0° tilt angle. The intensity for the (501) line plot continues to increase as the sample is tilted toward 90°. As the sample is tilted toward higher angles, more (501) crystal planes come into the proper orientation while (101) planes move out of the proper diffraction geometry.

These results indicate that the (101) planes of the MFI crystals in the molecular sieving layer are preferentially oriented at nearly 20° to the film surface while the (501) planes are preferentially oriented nearly perpendicular to the film surface. All crystals are not perfectly oriented because diffracted intensity spreads over a wide range of tilt angles. Crystals that are more highly oriented display sharper changes in diffracted intensity over a smaller range of tilt angles, as was seen in the case of zeolite A (Boudreau and Tsapatsis, 1997a,b). However, the X-ray pole-figure measurements of the (101) and (501) crystal planes for the MFI film confirm that the *preferred* orientation of the crystals in the molecular sieving layer is such that the *c*-axes of the crystals are oriented nearly perpendicular to the film surface. This means that the straight and sinusoidal channel networks are preferentially oriented parallel to the surface of the film. For a perfectly *c*-oriented MFI film (calcined), the (101) and (501) pole-figure line plots would be expected to exhibit intensity maxima at 34° and 73° tilt, respectively. At high tilt angles ($>60°$), deviations from these expected values and the results shown in Figure 2 could be attributed to defocusing effects. At lower tilt angles, defocusing is less of a concern and deviations from expected values (for example, the 20° maximum in the (101) pole-figure) are attributed to the morphology and growth process of the membrane and the presence of the randomly oriented layer of precursor crystals.

Figures 3a–3c show a series of FE-SEM and SEM micrographs from cross sections of the MFI membrane at various stages of secondary growth. Figure 3a (after 2 h secondary growth) shows that growing crystals emerge with many possible orientations during the early stages of secondary growth. These crystals are larger than the precursor particles but smaller than the crystal grains finally obtained. Moreover, it is evident that the growing crystals cover only a fraction of the surface of the precursor film. For longer heating times (6 h), shown in Figure 3b, the growing grains that were scattered across the surface became larger until they merged to eventually form a continuous thin layer with the orientation described above. Figure 3c shows the end result after 16 h secondary growth and illustrates the morphology of the intergrown layer, which consists of columnar grains oriented with their long dimension (*c*-axis) nearly perpendicular to the substrate.

Grains in a polycrystalline film with the highest vertical growth velocity with respect to the substrate surface will have the highest probability of survival (Van der Drift, 1967). As growth proceeds these grains will dominate the surface of the film. This type of "evolutionary selection" seems to be responsible for the oriented growth of the MFI membranes. At the earlier growth times, crystals of various orientations are present on the film surface. At later times, these grains intersect and grow into one another. Eventually, the grains with the fastest growth rate normal to the film and towards the nutrient source (i.e., the secondary growth solution) dominate at the surface, while others that grow more tilted become buried. For this case, the MFI crystals grow faster in the *c*-direction and the film microstructure as shown in Figure 3c is in agreement with this growth mechanism. The crystal grains near the surface of the film are more oriented in the *c*-direction than the crystal grains near the film/precursor interface.

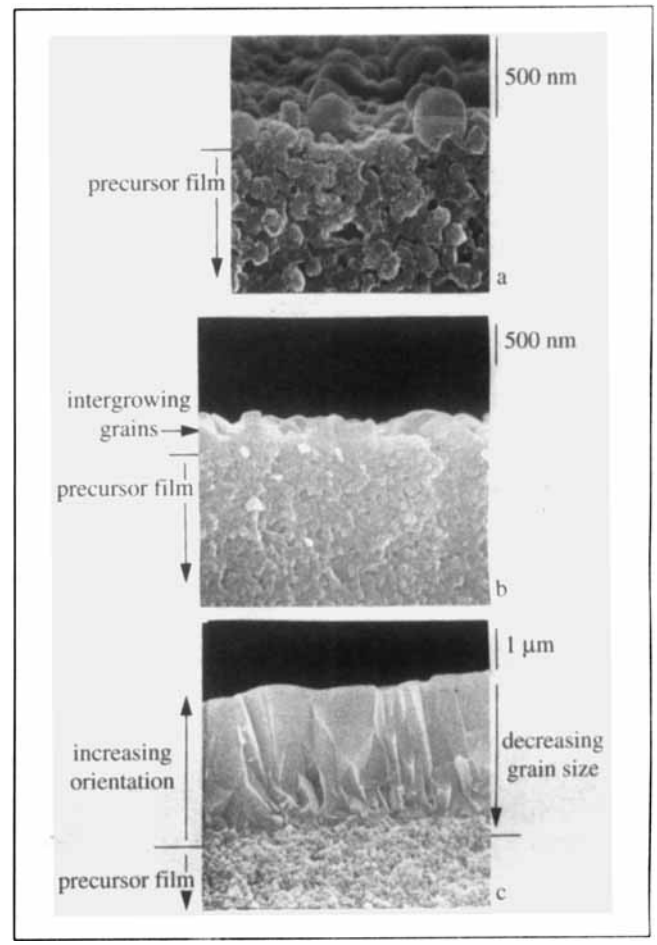

Figure 3. Cross sections of self-supported MFI film after secondary growth.

(a) FE-SEM 2-h heating, (b) SEM 6-h heating, (c) SEM 16-h heating.

We have been able to grow MFI films with thicknesses ranging from 0.5 μm to 100 μm. As shown in Figures 4a and 4b for a 7-μm and a 70-μm-thick film, respectively, these films consist of columnar grains. X-ray pole-figure measurements for these thicker films (Figure 4c) show much narrower orientation distribution of the *c*-axis around the surface normal. The (101) and (501) peaks, appearing at around 29° and 69° tilt respectively, are shifted closer to the expected tilt angles for perfectly *c*-oriented films while the (002) line plot, presented also in Figure 4c, shows maximum intensity at 0° tilt in agreement with the expected value for perfect *c*-orientation. This X-ray analysis indicates an increase of the orientation with the film thickness, which is consistent with the proposed growth mechanism.

The final product of secondary growth is an intergrown film.

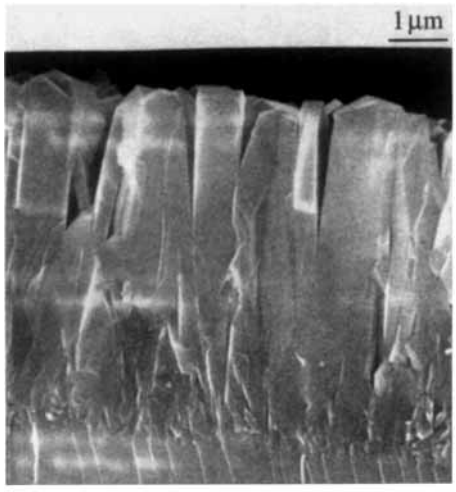

a

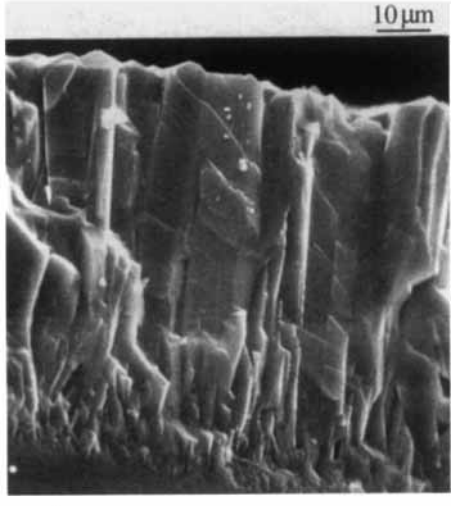

b

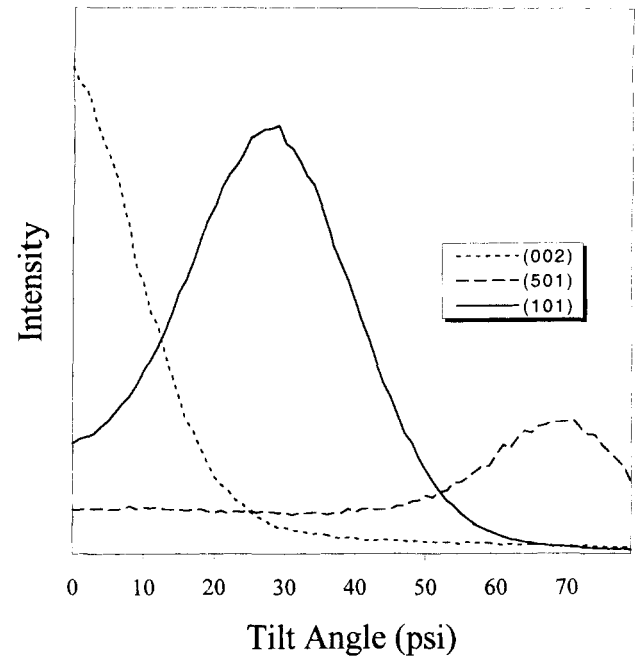

c

Figure 4. Thick supported MFI films.

(a) 7 μm thick, (b) 70 μm thick, and (c) XRD pole-figure analysis of film in Figure 4a.

Near the surface of this film, direct paths along the *c*-direction are available for transport. Approaching the precursor layer/zeolite film interface, the number of grains and grain boundaries increases while the degree of orientation decreases. Therefore, although the zeolite film is preferentially oriented it contains a buried region consisting of less ordered intergrown grains. Transport pathways exist within the crystal grains and between grain boundaries.

To investigate further the role of the precursor layer we performed a number of experiments by eliminating the use of the alumina binder from the silicalite suspension. The pure zeolitic suspension was used to coat glass slides with a precursor layer. In addition, the calcination step of the precursor film before secondary growth was omitted. Figure 5 shows the morphology of a typical film obtained after secondary growth of an uncalcined precursor layer deposited on a glass slide. The film consists of a more intergrown oriented layer of uniform thickness and of a smoother surface.

Figure 5c also shows a clear demonstration of the importance of the seed film. During dip coating the top part of the glass slide was not immersed in the zeolite suspension and therefore was left uncoated. Figure 5c shows a top view of the deposit morphology at the interface between the coated and uncoated region of the glass slide. The area not covered by the precursor film contains scattered crystals that are not intergrown well. In contrast, the regrown film is highly uniform with respect to orientation and crystal grain size. The film is optically transparent after secondary growth because of its uniformity, although its thickness well exceeds the wavelength of visible light. More details on the preparation of these transparent films and on microstructural manipulation during secondary growth are reported elsewhere (Gouzinis and Tsapatsis, 1998).

The role of calcination on the regrowth of precursor particles was demonstrated further by examining the behavior of a film that was subjected to an additional regrowth after secondary growth. Figures 6a and 6b show SEM top views of films that were calcined and not calcined before the final re-

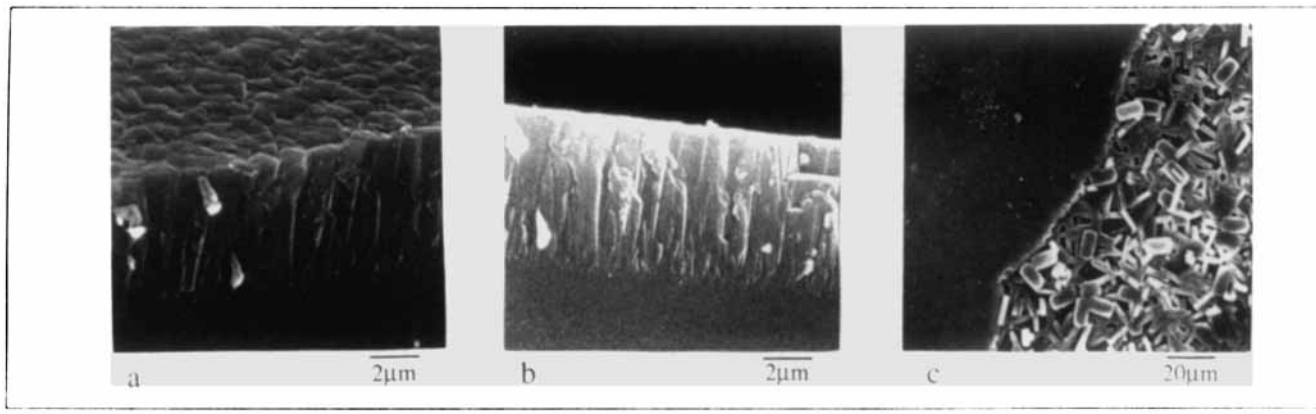

Figure 5. SEM view of optically transparent oriented MFI films on glass slides.
(a), (b) cross sections, (c) interface between coated (left) and uncoated (right) regions.

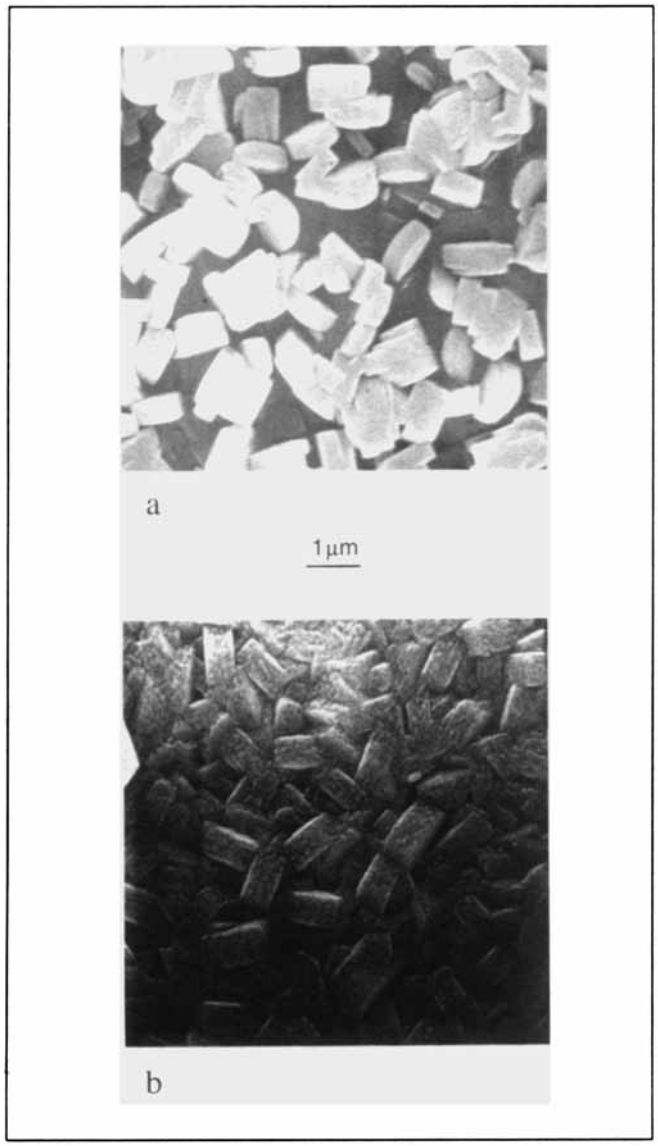

Figure 6. Calcination effects on the regrowth.
SEM top-views after second regrowth of (a) calcined films, and (b) uncalcined films.

growth, respectively. The calcined film (Figure 6a) has scattered *c*-oriented crystals deposited on the surface. The uncalcined film (Figure 6b) after the final regrowth exhibits a distinct morphology as a result of uniform growth of the existing crystals.

These results clearly demonstrate the role of the precursor layer for the formation of oriented and continuous films and also show that the history of the precursor layer (i.e., calcined or not, with or without additives) and its texture (nanocrystalline vs. microcrystalline) can greatly affect the secondary growth process. Consequently they point to systematic variation of the precursor layer as a means to manipulate the final film microstructure.

Supported membrane preparation

In what follows we limit our presentation to results from membranes prepared from calcined MFI/alumina composite precursor films, supported on porous alumina discs particles. Figure 7 shows a series of SEM photographs following a typical membrane-processing procedure. In Figure 7a, the polished alumina substrate shown is composed of large alumina particles (~ 1 μm) packed together, forming ~ 0.5-μm-sized pores. The substrate is coated with the silicalite particles until the entire surface is covered with the silicalite particles (Figures 7b and 7c).

The surface of the substrate is more rough compared to the zeolite particle size but this should not affect the secondary growth process and membrane formation as long as the particles completely cover the surface and are able to intergrow into a continuous membrane. Porous ceramic disks, with more smooth surfaces than the alumina disk used here, will be easier to coat with a continuous and smooth layer of precursor silicalite particles enhancing the success and reproducibility of the secondary growth procedure. The precursor layer must have an optimum thickness sufficient to completely cover the substrate but not so thick as to result in cracking or peeling. A thickness of 0.5 to 1 μm is preferred for the alumina substrates reported here. However, for flatter substrates this thickness can be reduced.

Figures 7d and 7e show SEM top-views of the alumina supported membrane after 16 h of secondary growth. The sur-

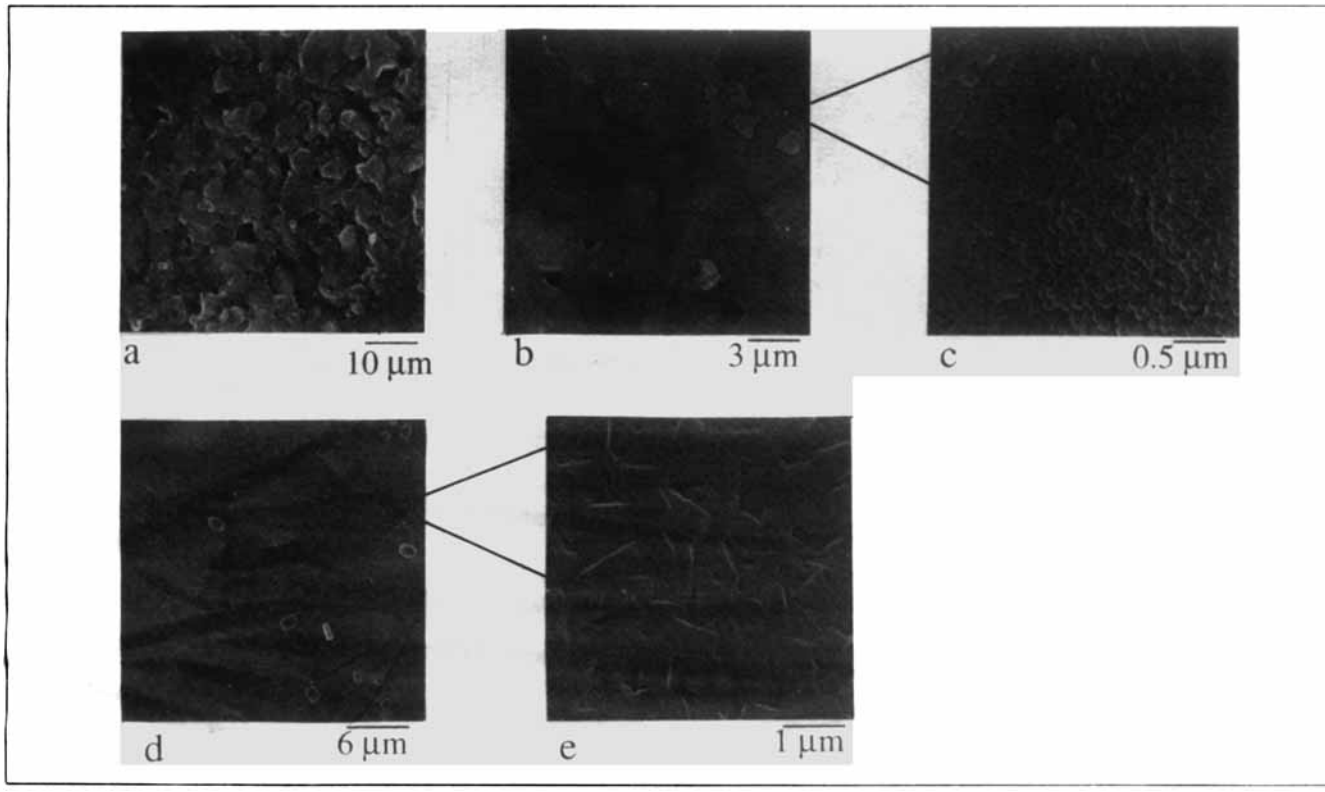

Figure 7. Preparation of a supported MFI membrane on porous alumina.

(a) SEM top-view of polished alumina substrate, (b) low-magnification SEM top-view of alumina substrate coated with silicalite nanocrystals, (c) high-magnification SEM top-view of alumina substrate coated with silicalite nanocrystals, (d) low-magnification top view of supported MFI membrane after 16 h secondary growth, and (e) high-magnification top view of supported MFI membrane after 16 h secondary growth.

face appears intergrown with the grain size at the surface being approximately 1 μm. An SEM cross section (Figure 8a) reveals that the thickness of the membrane is the same as the crystal grain size. The silicalite crystals forming the precursor film (~ 1 μm) lie under the molecular sieving layer which follows the contour of the porous substrate. This means that secondary growth does not occur by the deposition of multiple layers of crystals from solution. The same phenomena were observed in the preparation of similar unsupported and glass-supported films. The supported membranes have nearly the same microstructure as those previously reported. The crystals at the surface of the porous alumina-supported membrane appear to be oriented with both the straight and sinusoidal channel networks of the crystals nearly parallel to the film surface. Therefore, the porous alumina substrate once properly covered by silicalite seeds seems to have no pronounced effect on the membrane microstructure. Figure 8b shows another membrane prepared on a similar substrate with the same technique but with a thicker precursor film layer and longer secondary growth time. The resulting morphology of the intergrown layer is the same as that in Figure 8a although the precursor layer is several microns thick, which causes the film to peel or crack and thus makes it unsuitable for membrane applications. Thinner precursor films as shown in Figure 8a are preferred for this reason.

The rough surface of the membrane (caused by the roughness of the alumina substrate) prevents the use of XRD pole-figure analysis for more precise determination of the crystal orientation. However, as stated above on the basis of SEM results and comparison of unsupported films with glass-supported films, the local orientation is expected to be nearly the same as the one proposed for the glass-supported films in the previous section.

EDAX results for the alumina-supported membrane showed an average Si:Al ratio of ~ 23. This ratio varied at different regions on the surface. Because the surface of the supported membrane is rough and the intergrown layer is thin, a fraction of the Al signal may be attributed to the alumina substrate.

EDAX and EPMA analysis of self-supported membranes made with a precursor silicalite/alumina film showed no presence of Al in the surface layer. The self-supported membranes are smooth compared to the supported membranes and their analysis shows that evident leaching of Al from the binder into the top layer during secondary growth is not pronounced. Al nuclear magnetic resonance (NMR) measurements further support this view. After calcination and before secondary growth the precursor silicalite/alumina film has both tetrahedral and octahedral Al at a ratio of approximately 1:2. No change in this distribution of Al is observed by Al NMR after secondary growth. Also, the self-supported film surfaces were examined for the presence of Na using EPMA. Na is present in the precursor nanosilicalite particles, which was expected since Na was used for their synthesis. On the other hand, EPMA showed no presence of Na in the intergrown surface layer.

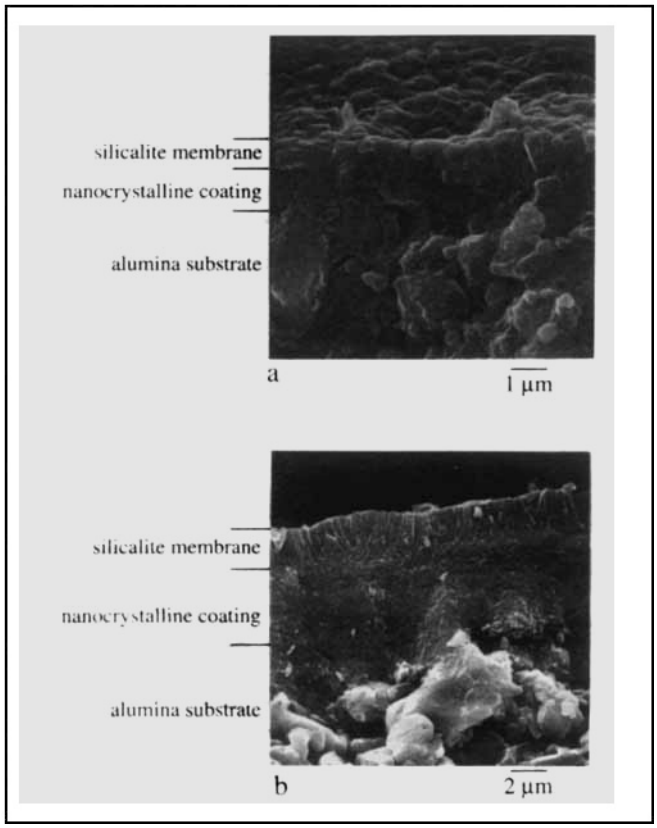

Figure 8. SEM cross-section of supported MFI membranes.

(a) MFI membrane No. 1 with thin precursor layer, and (b) MFI membrane No. 2 with thick precursor layer.

Permeation measurements

Single Gas Permeation. Figure 9 shows the single gas permeances of various gases plotted vs. inverse temperature on an Arrhenius-type plot for a membrane (MFI membrane No. 1). The trends seen in this figure correspond to those presented previously for a self-supported MFI membrane prepared with the same technique. Both cases show activated transport for all gases and high H_2/N_2 and O_2/N_2 selectivities compared to Knudsen-type selectivities. The permeances for the supported membrane are lower than those reported before, but this can be attributed to the thickness of the molecular sieving layer grown on the porous support (~ 1 μm) compared to the thickness of the molecular sieving layer for the self-supported membrane (~ 0.5 μm) or to the differences in the support resistances.

Table 1. Apparent Activation Energies for Gases Through MFI Membrane No. 1, Effective Radii, and Heats of Adsorption

	H_2	N_2	O_2	CH_4	CO_2
Ea (kJ/mol)	16 ± .5	24 ± 1	30 ± 1	22 ± .5	26 ± .5
Eff. radius (Å)		3.64	3.46	3.8	3.3
Q_{st} (kJ/mol)*		18		21	27

*Q_{st} is the isosteric heat of adsorption at 25°C from (Dunne et al., 1996)

Table 1 lists the apparent activation energies for the gases as determined from the Arrhenius plot along with the effective radii and heats of adsorption in silicalite for the various gases. The apparent activation energies are higher than typically reported data for other silicalite and ZSM-5 membranes as well as single crystal measurements but they are consistent with the values reported for the similar self-supported membrane (Lovallo and Tsapatsis, 1996). It should be noted that the measured apparent activation energies are close in value to reported heats of adsorption (Dunne et al., 1996) in silicalite.

Other supported MFI membranes were separately prepared using the same technique as described above. Figure 10 shows the permeation results for a membrane (MFI membrane number 2) prepared on the same type of substrate following the same procedure but showing different permeation

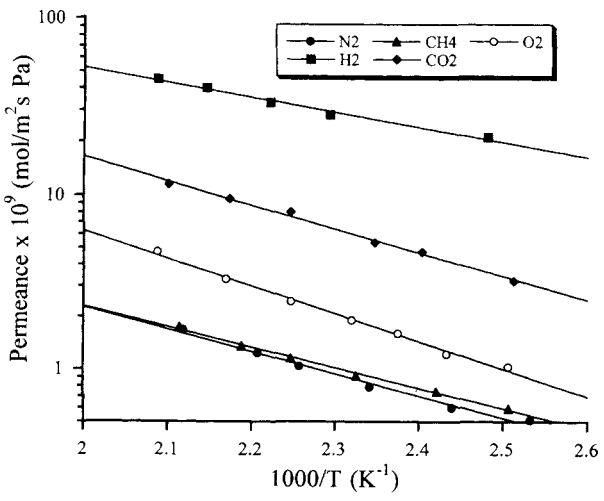

Figure 9. Single gas permeances for supported MFI membrane No. 1.

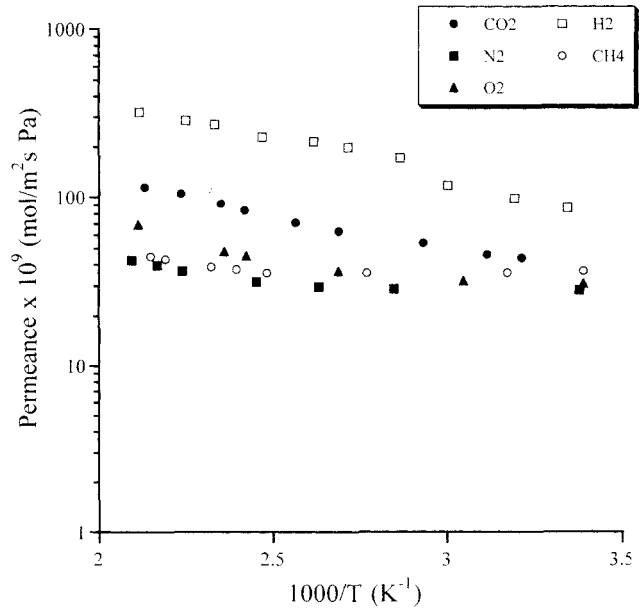

Figure 10. Single gas permeances for supported MFI membrane No. 2.

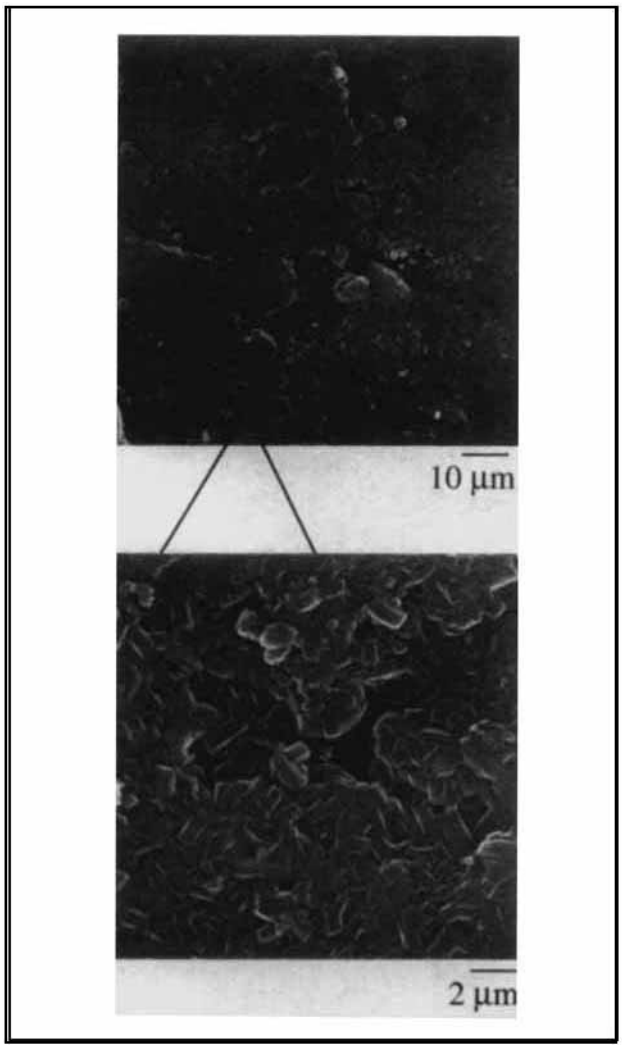

Figure 11. SEM top views of supported MFI membrane No. 2.

properties. The selectivities and apparent activation energies for this membrane are lower than for MFI membrane number 1. Moreover, the permeances are higher, indicating that the observed differences may be caused by a lower degree of intergrowth in the second membrane. Figure 11 shows SEM top-views of the membrane surface. The surface of this membrane is more rough than that of MFI membrane number 1, indicating a less intergrown surface, which may account for the differences in permeation properties. No large defects (~ 1 μm) were observed in the SEM. The two extremes of membrane, number 1 and number 2, show that at this time we do not have full control over the secondary growth of supported layers. Most likely substrate roughness influences the precursor quality, which in turn can influence the secondary growth process and the microstructure of the intergrown layer. Differences of the degree of intergrowth and film thickness result in differences in permselectivity and apparent activation energy. Membranes that exhibit superior selectivity show lower permeances and higher apparent activation energies.

Despite these difficulties related to substrate quality we have demonstrated the extension of the secondary growth procedure to supported films. The use of a porous substrate makes it possible to produce mechanically strong membranes with large areas. The procedure is not necessarily limited to alumina disks but may be extended to other inorganic tubes or plates like Vycor glass or stainless steel. The processing scheme is flexible enough to allow for membrane formation on a variety of substrates and various shapes. Other issues such as fine-tuning the reproducibility of the method, long-term stability during thermal cycling, membrane regeneration, and crack reparation still need to be addressed.

Mixed Gas Permeation. Permeation measurements of binary gas mixtures were carried out on self-supported MFI membranes similarly prepared with the secondary growth method (Lovallo and Tsapatsis, 1996) with a surface morphology comparable to that of the supported membrane described above and an intergrown layer thickness of ~ 0.5 μm as determined by SEM. The component permeances for the three binary mixtures were measured with respect to feed composition and temperature.

Figure 12 shows the binary permeation results for the gas pairs CO_2/N_2, O_2/N_2, and CO_2/CH_4, respectively. The data are plotted as the permeate vs. feed mole fraction of the faster permeating component. All three figures correspond well with the single gas measurements, that is, the membrane is more selective for CO_2 over CH_4, CO_2 over N_2, and O_2 over N_2.

Figure 13 shows results for the same gas pairs plotted as permeance vs. selective component feed composition. The permeances shown in this figure are lower (~ 30–40%) than those reported for single-gas measurements through self-supported membranes using pressure difference permeation (Lovallo and Tsapatsis, 1996). This can be attributed to the

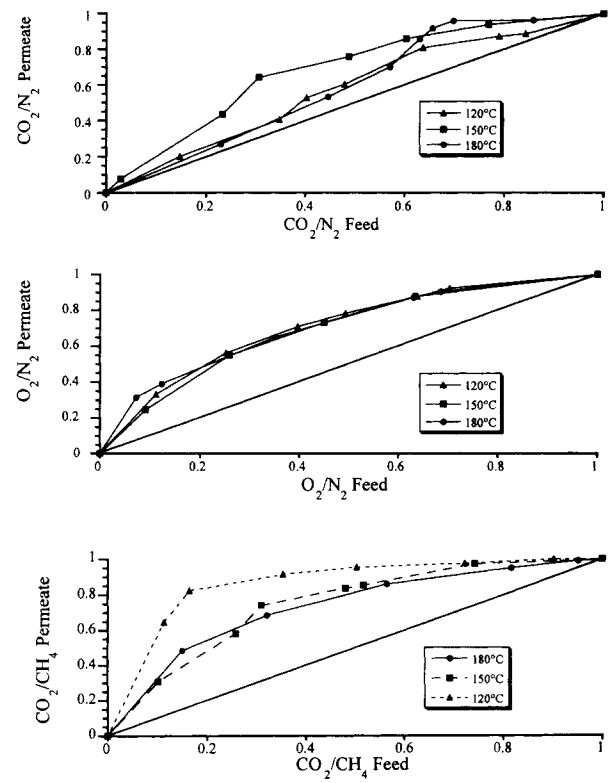

Figure 12. Binary gas permeation for supported silicalite membranes.

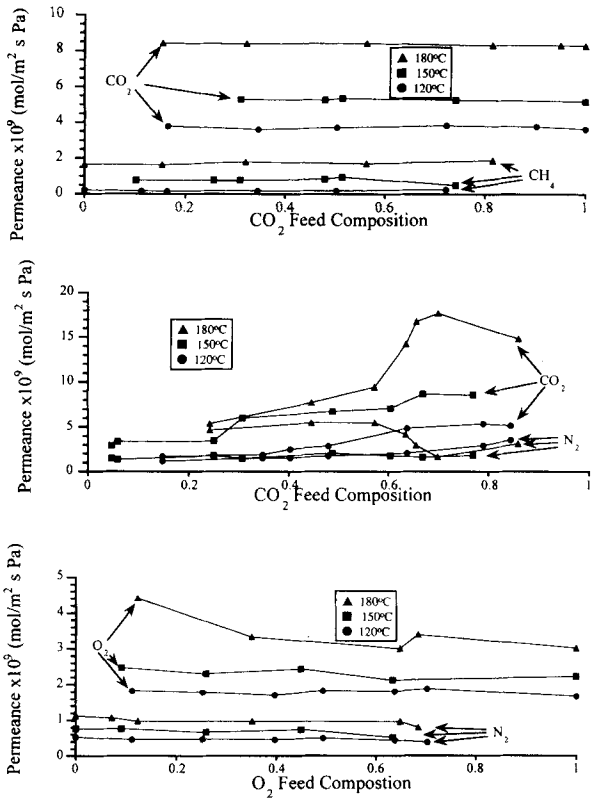

Figure 13. Binary gas permeances for supported MFI membranes.

back diffusion of He through the membrane from the sweep gas to the feed side. As can be seen in the figures, the permeance of all gases rises with temperature as expected from the single gas permeation data.

Discussion of Single and Mixed Gas Permeation Properties. From the single gas measurements, the supported membrane No. 1 displays ideal selectivities for H_2 over N_2 and CH_4 higher than 30 at 125°C, with permeances of 22.0, 0.5, and 0.7, (10^{-9} mol/m^2·s·Pa) respectively. The O_2 over N_2 selectivity is as high as 3.0 with permeances of 5.0 and 1.7 (10^{-9} mol/m^2·s·Pa) respectively. Also, the ideal selectivity for CO_2 over CH_4 is as high as 8 at 170°C with permeances of 9.0 and 1.1 (10^{-9} mol/m^2·s·Pa) respectively. These permeances are typically lower than those reported by other researchers for MFI-type membranes. Yan et al. (1995) reported values of 100, 40, and 73 (10^{-9} mol/m^2·s·Pa) for the permeance of H_2, N_2, and CH_4, respectively, through a ZSM-5 membrane at 185°C. Even larger values were claimed by Jia et al. (1994) with permeances of 1,560 and 4,400 (10^{-9} mol/m^2·s·Pa) for N_2 and H_2 in a supported silicalite membrane at 25°C. However, the membranes reported here are more selective for separations of these gases.

For the CO_2/CH_4 gas pair, decreasing temperature appears to increase the selectivity of the membrane more toward CO_2. In contrast, for the O_2/N_2 gas pair, the changing temperature has no effect on the selectivity of the membrane, while the CO_2/N_2 gas pair shows an increase and then a decrease of selectivity for CO_2 as temperature increases.

The CO_2/CH_4 mixture shows no change in permeance with feed composition. A similar trend is observed for O_2/N_2 although some variations in permeance are evident at higher temperatures for O_2. The CO_2/N_2 data show large changes in permeance as the CO_2 feed composition is increased, especially at elevated temperatures. As the CO_2 feed composition is raised, the CO_2 permeance increases and the N_2 permeance decreases. The CO_2/N_2 selectivity reaches values up to 20 at 180°C for mixtures with compositions larger than 60% in CO_2.

These observed single gas and binary permeation characteristics may be attributed to both transport and adsorptive features of the molecular sieving layer. All membranes display a selectivity for CO_2 over N_2 and CH_4 in single gas and binary measurements. Increased adsorptive strength and capacity for CO_2 in silicalite accounts for this observation. Reports of adsorptive strength for silicalite at room temperature follow the trend $CO_2 > CH_4 > O_2 \sim N_2$. Although the adsorptive characteristics of O_2 and N_2 are very similar in silicalite, as shown above, the membranes display a selectivity for O_2 over N_2. This feature indicates mobility differences for the two gases. Similarly, the relative CH_4 permeances do not follow adsorptive trends, suggesting a dominant transport effect.

The mobility effects can be related to the microstructure of the molecular sieving MFI layer. The orientation of the molecular sieving layer requires that diffusing species move between interconnecting channel networks in order to travel across the membrane. Molecules that move more easily between channel networks will display higher permeances. For separations occurring in the oriented portion of the membrane, the H_2 molecule may move more readily between channels than the larger N_2 molecule, accounting for the observed selectivity. A similar explanation may account for the observed selectivities for the O_2/N_2 and CH_4/N_2 pairs. Although the loading of the crystals might be nearly the same for O_2 and N_2, O_2 may move more readily across the membrane by switching between channel networks. In contrast, CH_4, although preferentially adsorbed with respect to N_2, displays an overall reduced permeance because of reduced mobility.

In addition to these observations, for the most selective membranes, we observed a high apparent activation energy for permeation. The adsorption of larger organic molecules on the zeolite surface from impurities in the atmosphere, feed streams, or epoxy may influence the permeation properties of these devices. Funke et al. (1997) have recently reported on such effects using *n*-octane and 1,3,5-trimethyl benzene on silicalite membranes. However, this does not seem to be a possible explanation here for the gases measured and the temperature range investigated.

A possible explanation for the unusually large activation energy of the membranes is based on their microstructure and small thickness. The membranes are composed of many crystal grains that are more oriented and larger at the membrane surface with decreasing orientation and grain size toward the MFI layer/precursor film interface. Transport through a single grain involves adsorption at the external surface, surface diffusion and entrance in the interior of the grain, intercrystalline transport, exit from the crystal interior, and desorption. Barrer (1990) introduced a model to account for surface resistances vs. intercrystalline transport for a single crystal. This research showed that, depending on the en-

ergies of the surface processes, surface resistances (i.e., desorption from the crystal interior) may become rate-limiting for small crystals and/or low temperatures. For the films reported here a number of grain boundaries will be encountered by a molecule as it moves through the membrane and therefore additional adsorption/desorption steps within the membrane will be introduced. These additional steps may increase the role of surface resistances on permeation properties. In the temperature regimes measured here and because of the small thickness of the membrane, desorption resistance at the crystal grain boundaries across the membrane may be responsible for the high apparent activation energies (Table 1). The close correspondence of apparent activation energies to heats of adsorption corroborates this hypothesis.

Further studies are underway in order to clarify the effects of membrane microstructure (thickness, grain size, degree of orientation) on permeation properties.

Conclusions

Secondary growth of precursor nanocrystalline films has been successfully implemented on porous alumina substrates. The membranes exhibit characteristics and have a microstructure consistent with previous results from similarly prepared self-supported membranes. New results for permeation of CO_2 and CH_4 reveal an ideal selectivity for CO_2 over CH_4 as high as 10 and H_2 over CH_4 as high as 30. Binary feed permeances follow trends of single gas permeances. The permeance of the CO_2/N_2 gas pair is influenced more from the feed composition than the other gas pairs. Both adsorption/desorption and diffusion seem to influence the observed permeances, selectivities and activation energies that are attributed to the microstructure of the molecular sieving layer.

X-ray pole-figure analysis has confirmed the proposed preferred orientation of the MFI layer. The crystal grains are preferentially oriented with both straight and sinusoidal channel networks parallel to the membrane surface and the degree of orientation increases along the membrane thickness. EDAX and EPMA have shown that the intergrown top layer on self-supported films consists of pure silica MFI.

Acknowledgment

Support for this work was provided by NSF [CTS-9624613 (CAREER) and CTS-9512485 (ARI)]. M.T. is grateful to the David and Lucile Packard Foundation for a Fellowship in Science and Engineering. We also acknowledge the W. M. Keck Polymer Morphology Laboratory for use of its Electron Microscopy facilities.

Literature Cited

Bakker, W. J. W., F. Kapteijn, J. Poppe, and J. A. Moulijn, "Permeation Characteristics of a Metal-Supported Silicalite-1 Zeolite Membrane," *J. Memb. Sci.*, **117**, 57 (1996).

Barrer, R. M., "Porous Crystal Membranes," *J. Chem. Soc. Faraday Trans.*, **86**, 1123 (1990).

Boudreau, L. C., and M. Tsapatsis, "A Highly Oriented Thin Film of Zeolite A," *Chem. Mat.*, **9**, 1705 (1997a).

Boudreau, L. C., J. A. Kuck, and M. Tsapatsis, "Deposition of Oriented Zeolite A Films: In-situ and Secondary Growth," *J. Memb. Sci.*, (1997b, in press).

Dunne, J. A., R. Mariwala, M. Rao, S. Sircar, R. J. Gorte, and A. L. Myers, "Calorimetric Heats of Adsorption and Adsorption Isotherms," *Langmuir*, **12**, 5888 (1996).

Funke, H. H., K. R. Frender, K. M. Green, J. L. Wilwerding, B. A. Sweitzer, J. L. Falconer, and R. D. Noble, "Influence of Adsorbed Molecules on the Permeation Properties of Silicalite Membranes," *J. Memb. Sci.*, **129**, 77 (1997).

Geus, E. R., J. E. Marcel, and H. Bekkum, "Synthesis and Characterization of Zeolite (MFI) Membranes on Porous Ceramic Supports," *J. Chem. Sci. Faraday Trans.*, **88**, 3101 (1992).

Gouzinis, A., and M. Tsapatsis, "On the Preferred Orientation and Microstructural Manipulation of Molecular Sieve Films Prepared by Secondary Growth," *Chem. Mat.*, in press.

Huijser-Gerits, E. M. C., and G. D. Rieck, "Defocusing Effects in the Reflection Technique for the Determination of Preferred Orientation," *J. Appl. Crystallog.*, **7**, 286 (1974).

Jia, M. D., K. V. Peinemann, and R. D. Behling, "Ceramic Zeolite Composite Membranes," *J. Memb. Sci.*, **82**, 15 (1993).

Jia, M. D., B. Chen, R. D. Noble, and J. L. Falconer, "Ceramic-Zeolite Composite Membranes and their Application for Separation on Vapor/Gas Mixtures," *J. Memb. Sci.*, **90**, 1 (1994).

Kapteijn, F., W. J. W. Bakker, J. Van De Graaf, G. Zheng, J. Poppe, and J. A. Moulijn, "Permeation and Separation Behavior of a Silicalite-1 Membrane," *Catal. Today*, **25**, 213 (1995).

Kusakabe, K., T. Kuroda, A. Murata, and S. Morooka, "Formation of a Y-type Zeolite Membrane on a Porous Alpha-Alumina Tube for Gas Separation," *Ind. Eng. Chem. Res.*, **36**, 649 (1997).

Lai, W. F., H. W. Deckman, J. A. McHenry, and J. P. Verduijn, "Zeolite Layers with Controlled Crystal Width and Preferred Orientation Grown on a Growth Enhancing Layer," *International Patent Application*, WO 96/01687 (1996).

Lovallo, M. C., M. Tsapatsis, and T. Okubo, "Preparation of an Asymmetric Zeolite L Film," *Chem. Mat.*, **8**, 1579 (1996a).

Lovallo, M. C., L. Boudreau, and M. Tsapatsis, "Preparation of Supported Zeolite Films and Layers: Processing of Zeolite Suspensions and In-situ Growth from Homogeneous Solutions," *Microporous and Macroporous Materials*, J. S. Beck, L. E. Iton, L. E. Corbin, R. F. Lobo, M. E. Davis, S. I. Zones, and S. L. Suib, eds., MRS, Pittsburgh, **431**, 225 (1996b).

Lovallo, M. C., and M. Tsapatsis, "Microstructural Characterization of an Oriented Silicalite Film," *Advanced Catalytic Materials III*, P. Lendor, M. Ledoux, D. Nagaki, and L. Thompson, eds., MRS, Pittsburgh, in press (1998).

Lovallo, M. C., and M. Tsapatsis, "Preferentially Oriented Submicron Silicalite Membranes," *AIChE J.*, **42**, 3020 (1996).

Mintova, S., J. Hedlund, B. Schoeman, V. Valtchev, and J. Sterte, "Continuous Films of Zeolite ZSM-5 on Modified Gold Surfaces," *Chem. Commun.*, **15** (1997).

Noble, R. D., and J. L. Falconer, "Silicalite-1 Zeolite Composite Membranes," *Catal. Today*, **25**, 209 (1995).

Tsapatsis, M., T. Okubo, M. C. Lovallo, and M. E. Davis, "Synthesis and Structure of Ultrafine Zeolite KL (LTL) Crystallites and Their Use for Thin Film Zeolite Processing," *Mat. Res. Soc. Symp. Proc.*, **371**, 21 (1995a).

Tsapatsis, M., M. C. Lovallo, T. Okubo, M. E. Davis, and M. Sadakata, "Characterization of Zeolite L Nanoclusters," *Chem. Mat.*, **7**, 1734 (1995b).

Tsikoyiannis, J. G., and W. O. Haag, "Synthesis and Characterization of a Pure Zeolitic Membrane," *Zeolites*, **12**, 126 (1992).

Valtchev, V., B. J. Schoeman, J. Hedlund, S. Mintova, and J. Sterte "Preparation and Characterization of Hollow Fibers of Silicalite," *Zeolites*, **17**, 408 (1996).

Van der Drift, A., "Evolutionary Selection, a Principle Governing Growth Orientation in Vapor-Deposited Layers," *Philips Res. Rep.*, **22**, 267 (1967).

Vroon, Z. A. E. P., K. Keizer, M. J. Gilde, H. Verweij, and A. J. Burggraaf, "Transport Properties of Alkanes Through Ceramic Thin MFI Membranes," *J. Memb. Sci.*, **113**, 293 (1996).

Yan, Y., M. Tsapatsis, G. R. Gavalas, and M. E. Davis, "Zeolite ZSM-5 Membranes on Porous α-Al_2O_3," *J. Chem. Soc. Chem. Commun.*, 227 (1995).

Yee, A. L., H. C. Ong, L. M. Stewart, and R. P. Chang, "Development of Flat, Smooth (100) Faceted Diamond Thin Films Using Microwave Plasma Chemical Vapor Deposition," *J. Mat. Res.*, **12**, 1796 (1997).

Manuscript received Nov. 21, 1997, and revision received May 28, 1998.